International Communications in Heat and Mass Transfer 126 (2021) 105473

Contents lists available at ScienceDirect

International Communications in Heat and Mass Transfer

journal homepage: www.elsevier.com/locate/ichmt

An analytical fractal model for permeability in isotropic open-cell metal foam with surface roughness

Tian Xiao [a], Junfei Guo [b], Gang Liu [b], Xiaohu Yang [b,*], Tian Jian Lu [c,d,**]

[a] State Key Laboratory for Strength and Vibration of Mechanical Structures, School of Aerospace, Xi'an Jiaotong University, Xi'an 710049, PR China
[b] Institute of the Building Environment & Sustainability Technology, School of Human Settlements and Civil Engineering, Xi'an Jiaotong University, Xi'an 710049, PR China
[c] State Key Laboratory of Mechanics and Control of Mechanical Structures, Nanjing University of Aeronautics and Astronautics, Nanjing 210016, PR China
[d] MIIT key Laboratory of Multifunctional Lightweight Materials and Structures (MLMS), Nanjing University of Aeronautics and Astronautics, Nanjing 210016, PR China

ARTICLE INFO

Keywords:
Permeability
Surface roughness
Fractal analysis
Open-cell metal foam
Direct numerical simulation

ABSTRACT

This paper develops analytically a fractal model for estimating flow permeability of open-cell foam with rough surfaces. Fractal theory is employed for better characterize the randomness of pore distribution in the porous media and for describing particularly the micro roughness on the metallic ligaments. This provides a closer look at the actual situation of pore distribution of open-cell foams. The permeability can mainly be expressed with porosity, average tortuosity, and micro-rods geometric parameters, without any empirical or fitting parameters. The analytical model is verified through comparison to existing experimental data. To further explain the influence of micro-rods on the permeability, a tetradecahedral unit cell is used for pore-scale simulation. It is found that the reduced permeability is caused mainly by the increased flow tortuosity and the surface friction between fluid transport and the micro roughness.

1. Introduction

Open-cell metal foam enjoys the superiorities of high porosity, light weight, large specific area, and fluid mixing capability, and it has been widely involved in a broad range of engineering applications such as thermal management of electronics devices [1], chemical catalyst [2,3], fuel cells [4,5], thermal energy storage [6,7] and biomedical applications [8,9]. Fluid flow and convective heat transfer are the key processes in these applications. The large surface area and strong flow mixing capability for metal foam are the predominated contributors to heat transfer enhancement. To characterize metal foam for thermal engineering applications, except for heat transfer coefficient, flow resistance (pressure drop) should also be given considerable attentions. Microscopically, it is essential to understand the transport phenomena in porous media at pore scale; Macroscopically, the characterization of permeability serves the physical basis for utilizing open-cell metal foams since permeability quantitatively justifies the fluid transport in porous media.

Fluid flow phenomena and permeability depend on the intrinsic microstructure of individual porous medium [10–12]. To determine permeability, characterization of porous microstructure paves the foundation for transport physics. Since open-cell metal foam consists of randomly-distributed metallic ligaments, forming inter-connected pore space, directly solving Navier-Stokes equations seems impossible. To this end, the complicated porous structure is assumed to be periodically distributed and unit cell (UC) or part of UC is formed to represent both the topology and morphology for the bulk porous medium, under which condition the macroscopic flow problem is solved by performing the volume-averaged manipulation on the pore-scale Navier-Stokes equations [13,14].

Via modifying Kozeny-Carmen model, spherically-packed bed UC was employed to predict the permeability of metal foam. Good agreement can be obtained with fitting empirical constants [15–18]. However, packed spheres seemed inappropriate for representing porous matrix for metal foam and the fluid flow characteristics between packed beds and foam were significantly different. To account for the effect of metal foam microstructure, a cubic lattice truss structure seemed more suitable. Based on this microstructure, continuous studies were conducted on determining permeability. Du Plessis et al. [19] proposed an

* Corresponding author.
** Corresponding author at: Institute of the Building Environment & Sustainability Technology, School of Human Settlements and Civil Engineering, Xi'an Jiaotong University, Xi'an 710049, PR China.
E-mail addresses: xiaohuyang@xjtu.edu.cn (X. Yang), tjlu@nuaa.edu.cn (T.J. Lu).

https://doi.org/10.1016/j.icheatmasstransfer.2021.105473

Available online 15 July 2021

Nomenclature

Symbols

A	Cross - sectional area (m^2)
c	Micro - rods surface distance (m)
d	Pore size(m)
d_E	Euclidean dimension
D_f	Fractal dimension of the pore size distribution
D_T	Fractal dimension of average tortuosity
h	Height of micro-rods (m)
$\overline{h}_\lambda$	Equivalent height of micro-rods (m)
K	Permeability (m^2)
L	Measurement scale (m)
L_0	Characteristic length (m)
N	Number of pores
P	Pressure (Pa)
q	Volume Flowrate (m^3/s)
Q_R	Total volume Flowrate (m^3/s)
r	Radius of micro-rods (m)
S	Surface area (m^2)
t	Center distance of micro-rods(m)
t_s	Ligament thickness(m)
V	Volume (m^3)
V_{total}	Total volume (m^3)
V_{pore}	Pore volume (m^3)

Greek symbols

β	Dimensionless roughness
ω	Distribution density of micro-rods
μ	Dynamic viscosity (Pa · s)
λ	Pore diameter (m)
ε	Porosity
τ	Tortuosity

Subscript

av	Average
max	Maximum
min	Minimum
R	Rough surface
RS	Representative structure
t	Total

analytical model that can give a quite good prediction for permeability in a very high porosity range (0.973 – 0.978).Bhattacharya et al. [20] then extended their model with a fitting correlation of determining node size for cubic UC. With their extension, the modified model worked well in a wider porosity range (0.90 – 0.98). However, Ahmed et al. [21] later found a physically impossible increment in flow tortuosity with porosity in Bhattacharya et al.'s model. They attempted to further correct and modify the cubic UC model by introducing a non-constant node size, which successfully predicted permeability and flow tortuosity as a function of porosity. Based on the cubic UC with spherical nodes, Yang et al. [22] analytically proposed a prediction model for foam permeability and the results demonstrated a good agreement with experimental data.

The structure of the metal foam is spatially disordered, but it essentially follows the fractal theory. Fractal analysis on the microstructure of metal foam may provide a better solution to characterize the complex inner-connected porous matrix, favoring determining permeability and understanding the flow processes at the pore scale. Particularly, the fractal theory is good at characterizing the surface microroughness at the pore scale [23–26]. This seems coincidental to be a distinct solution to analyze fluid flow in surface roughed metal foam that was fabricated by Ren et al. [27,28] very recently. The fractal theory assumes that the pore distribution, pore size and pore shape follow the fractal scaling law and the pore-scale flow paths are also treated as a bundle of tortuous capillaries. Permeability can be analytically determined with the help of fractal dimensions for size distributions of capillaries and flow tortuosity.

Yu and Cheng [29] introduced the fractal distribution of capillaries into the capillary bundle model, and they developed an analytical expression for permeability for bi-dispersed porous medium. Their model was demonstrated to have non-empirical constants. This work laid the physical basis for the continuous explorations on permeable transport flow in fractal porous media. Yu et al. [30] characterized the pore shapes inside four different glass fiber preforms and proposed an analytical expression for fractal in-plane permeability. The fractal model was able to consider the influence of compression on the porosity changes of fiber preforms. Shou et al. [31] accounted for the discrete and discontinuous nature of fractal porous media and developed a difference-fractal model for estimating permeability of fibrous porous media. Difference approach was used to develop the fractal model. Besides, Shen et al. [32] tried another way to improve the fractal model for permeability via the pore-filling method. Their model was shown to estimate the fractal porosity and pore volume distribution and this favored the probability of density function for pore size without conventional restrictions. Xiao et al. [33] characterized the porous layer of gas diffusion by porosity, tortuosity fractal dimension, pore area fractal dimensions, and etc. Based on these fractal characteristics, an analytical expression of predicted dimensionless permeability was developed and was shown to agree well with experimental results. Cai and Yu [34] justified the contribution of the maximum pore size in fractal porous media and two analytical models were developed. It was demonstrated that permeability was significantly reduced as a decrease in the maximum pore size. Previous scholars continuously contributed to the development of transport flow in fractal porous media. More details can be referred to the recent review work of Cai et al. [35] and Xu et al. [36]

It needs to be mentioned here that all of the aforementioned models deal with porous media with smooth surface. As for the roughed surfaces, Majumdar and Bhushan [37] employed fractal theory to characterize the size distribution of contact areas on the roughness surface and this size distribution (W-M function) was widely used in the determination of the micro fractal roughness morphology in the continuous studies [38,39]. Yang et al. [40] developed an analytical fractal model to predict the pressure gradients, friction factors, and Poiseuille numbers in roughed channels. Geometric characterization of cone-like rough elements was performed by fractal theory and an analytical expression for relative roughness was derived. Later, Yang et al. [41] continued to establish a fractal attempt to estimate permeability of porous media with cone-like rough elements on the surface. Their model indicated that the permeability followed a quadruplicate power law of the relative roughness. Recently, a fractal model for modeling flow resistance of laminar flow through tree-like branching networks with cone-like rough elements was developed [41]. It demonstrated that the total pressure drop across a tree-like branching network with roughened channels was increased by a quadruplicate power law of relative roughness but permeability was decreased by a square one. Besides the aforementioned progress in fractal theory for modeling transport in porous media, numerical simulations such as Molecular Dynamic Method [42], Lattice Boltzmann Method [43], Monte Carlo Simulation [44] have been recently applied to solve 3D Navier-Stokes equations at the pore scale.

To be conclusive, previous investigations contributed to the development of fractal theory on understanding transport phenomena in porous medium and predicting its permeability. The effect of surface roughness on flow characteristics and permeability has been intensively studied. At present, however, little attention has been paid to

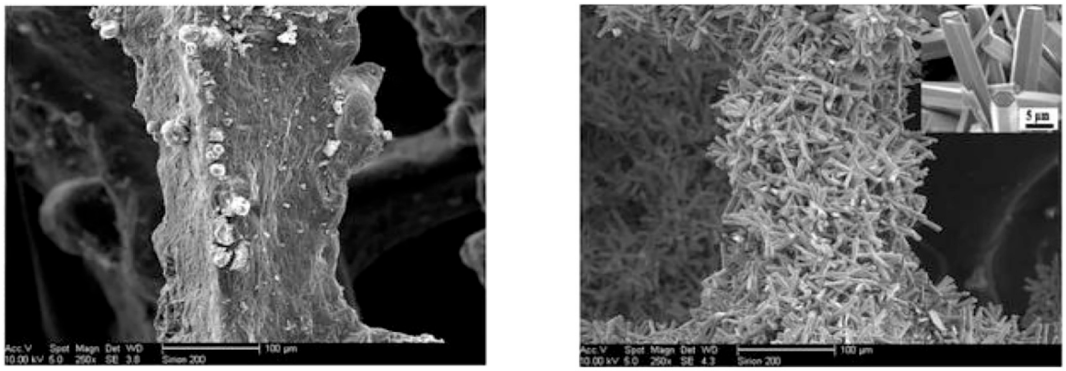

Fig. 1. (a) SEM image of the original metal foam ligament [27]; (b) SEM image of a ligament with micro-rods [27].

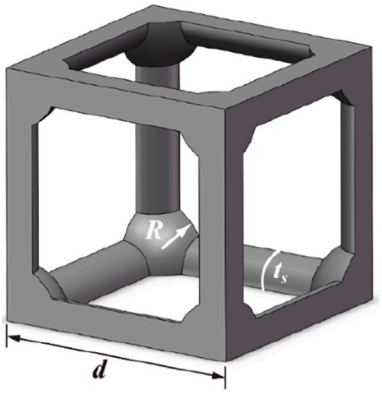

Fig. 2. Open-cell foam with smooth surface and node.

analytically predict the permeability of open - cell metal foam with rough surfaces using fractal theory. Besides, the justification of the contribution of surface roughness to flow features inside open-cell metal foam or the development of predicting model for permeability using fractal theory remain elusive. To this end, this paper aims to employ fractal theory to squarely address this issue, trying to provide physical insights into the transport phenomena in open-cell metal foam. Pore-scale geometric characterization is performed and fractal model for metal foam permeability is determined. Experimental results and pore-scale numerical simulations on the permeability of metal foam (smooth and rough surface) are employed for validating the fractal model. The effects of length and radius of micro-rods on permeability are explored, as well.

2. Theoretical model

2.1. Theory for fractal porous media

It has been shown that the shape, size and distribution of pores satisfy the fractal law in porous media [45]. When the size of pores is greater than λ, the fractal relationship between the number of pores N and the pore size λ is as follows [29]:

$$N(L \geq \lambda) = (\lambda_{\max}/\lambda)^{D_f} \tag{1}$$

where D_f is the fractal dimension of fractal porous media, $\lambda_{\max}$ is the maximum pore size of the porous medium, L is the measurement scale, and $N(L \geq \lambda)$ is the total number of pores that their pore sizes are not less than λ. When the pore size λ is replaced by minimum pore diameter $\lambda_{\min}$, the total number of pores N_t can be expressed as [29]:

$$N_t = (\lambda_{\max}/\lambda_{\min})^{D_f} \tag{2}$$

where $\lambda_{\min}$ denotes the minimum pore size of the porous medium.

The pore size distribution of porous media is discontinuous in practice. In general, there are a lot of pores in a unit volume for porous media. Therefore, the fractal scale law (Eq. (1)) between the number of pores and the size of pores is approximately continuous and differentiable. The number of pores in the infinitesimal range of λ to $\lambda + d\lambda$ can be obtained by differentiating λ in Eq. (1) [29,30,46].

$$-dN = D_f \lambda_{\max}^{D_f} \lambda^{-(D_f+1)} d\lambda \tag{3}$$

Dividing Eq. (3) by Eq. (2) gives:

$$-\frac{dN}{N_{total}} = D_f \lambda_{\min}^{D_f} \lambda^{-(D_f+1)} d\lambda = f(\lambda) d\lambda \tag{4}$$

where $f(\lambda) = D_f \lambda_{\min}^{D_f} \lambda^{-(D_f+1)}$ is the probability density function for pores in fractal porous media [29,47]. According to probability theory, the integral of the probability density function has the following relationship [29,47].

$$\int_{-\infty}^{+\infty} f(\lambda) d\lambda = \int_{\lambda_{\min}}^{\lambda_{\max}} f(\lambda) d\lambda = 1 - \left(\frac{\lambda_{\min}}{\lambda_{\max}}\right)^{D_f} \equiv 1 \tag{5}$$

If and only if

$$\left(\frac{\lambda_{\min}}{\lambda_{\max}}\right)^{D_f} \cong 0 \tag{6}$$

For Eq. (6), Yu and Li [47] thought the relationship is a key basis for using fractal geometry theory to deal with porous media. And based on the Sierpinski carpet and Sierpinski sponge model, the fractal dimension of fractal porous media is obtained as [47]:

$$D_f = d_E - \frac{ln\varepsilon}{ln(\lambda_{\min}/\lambda_{\max})} \tag{7}$$

where d_E is Euclidean dimension ($d_E = 2$ denotes the two-dimensional space and $d_E = 3$ represents the three-dimensional space), ε is the porosity of porous media. In the two-dimensional space, $0 < D_f < 2$; and in the three-dimensional space, $0 < D_f < 3$.

Eqs. (1)–(7) are the theoretical basis of fractal geometry for porous media.

2.2. The permeability model of foam with rough surfaces

Thanks to the method of fabrication, the surface of the ligament is not smooth. Ren et al. [27] prepared ZnO micro-rods on the wall of open-cell aluminum foam cells by the hydrothermal method (as shown in Fig. 1). These micro-rods increase the roughness and surface area for

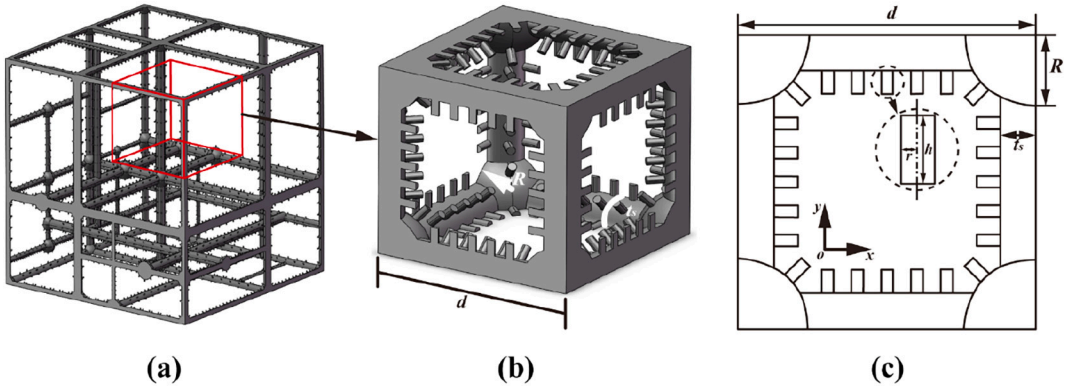

Fig. 3. A modified cubic model with cylinder micro-rods on the surface: (a) Porous structure with surface roughness; (b) 3D UC model; (c) Top view.

the open-cell metal foam. Under this situation, the original smooth cubic unit cell is no longer applicable (as shown in Fig. 2). To describe the influence of micro-rods on fluid transport characteristics, the original cubic unit cell model needs to be modified accordingly. Therefore, a new cubic UC model with periodic cylindrical micro-rods covering the surfaces is developed (as shown in Fig. 3). In the following model development sections, the modified cubic UC with micro-rods on the ligaments is employed and analyzed.

2.2.1. Fractal model for permeability

The volumetric flow of fluid $q(\lambda)$ through a single tortuous circular tube satisfies the modified Hagen-Poiseulle formula [48].

$$q(\lambda) = \frac{\pi}{128}\frac{\lambda^4 \Delta P}{\mu L_t(\lambda)} \tag{8}$$

where μ denotes the dynamic viscosity of fluid, ΔP denotes the pressure drop, $L_t(\lambda)$ represents the actual length of the tortuous tube. Compared to open-cell metal foams with smooth surfaces, the hydraulic diameter of a cubic UC covered with micro-rods is relatively reduced. Therefore, Eq. (8) needs to be modified to make it suitable for open-cell metal foams with rough surfaces. It is necessary to modify the size of channel through replacing the size λ with the size $\lambda - 2\bar{h}_\lambda$.

$$q_R\left(\lambda\text{-}2\bar{h}_\lambda\right) = \frac{\pi}{128}\frac{\left(\lambda\text{-}2\bar{h}_\lambda\right)^4 \Delta P}{\mu L_t\left(\lambda - 2\bar{h}_\lambda\right)} = \frac{\pi}{128}\frac{\lambda^4 \Delta P}{\mu L_t\left(\lambda - 2\bar{h}_\lambda\right)}(1-\beta)^4 \tag{9}$$

And

$$L_t\left(\lambda - 2\bar{h}_\lambda\right) = \left(\lambda - 2\bar{h}_\lambda\right)^{1-D_T} L_0^{D_T} = \lambda^{1-D_T}\left(1 - 2\bar{h}_\lambda \Big/ \lambda\right)^{1-D_T} L_0^{D_T} \tag{10}$$

where $\bar{h}_\lambda$ is the equivalent height of micro-rods, $q_R\left(\lambda\text{-}2\bar{h}_\lambda\right)$ presents the flow through a single tortuous circular tube with rough surface, and $\beta = 2\bar{h}_\lambda/\lambda$ denotes the roughness. The total volumetric flow Q_R through the unit cross-section can be calculated by summing the flow rates of all tortuous tubes.

$$\begin{aligned} Q_R &= -\int_{\bar{\lambda}_{\min}}^{\bar{\lambda}_{\max}} q_R\left(\lambda - 2\bar{h}_\lambda\right) dN \\ &= \frac{\pi}{128}(1-\beta)^{3+D_T}\frac{1}{\mu {L_o}^{D_T}}\frac{\Delta P D_{f,3}\bar{\lambda}_{\max}^{3+D_T}}{3 - D_{f,3} + D_T}\left[1 - \left(\frac{\bar{\lambda}_{\min}}{\bar{\lambda}_{\max}}\right)^{3-D_{f,3}+D_T}\right] \end{aligned} \tag{11}$$

where $1 < D_T < 3$ and $1 < D_{f,3} < 3$. Therefore, this formula of $3 - D_{f,3} + D_T > 1$ is satisfied. According to Eq. (6), it is obtain that $\left(\bar{\lambda}_{\min}/\bar{\lambda}_{\max}\right)^{3-D_f+D_T} \approx 0$. Then Eq. (11) is simplified to be:

$$Q_R = \frac{\pi}{128}\frac{1}{\mu {L_o}^{D_T}}\frac{\Delta P D_{f,3}}{3 - D_{f,3} + D_T}\bar{\lambda}_{\max}^{3+D_T}(1-\beta)^{3+D_T} \tag{12}$$

where L_0 depicts the length of the straight channel, D_T represents the fractal dimension of the average tortuosity, and $\bar{\lambda}_{\max}$ denotes the maximum pore size of porous media with rough surface. Combining Eq. (12) with Darcy law ($Q_R = \frac{K_R \Delta P A}{\mu L_0}$), the expression of the permeability of porous media with rough surface can be obtained as:

$$K_R = \frac{\pi}{128}\frac{{L_0}^{1-D_T}}{A}\frac{D_{f,3}}{3 - D_{f,3} + D_T}\bar{\lambda}_{\max}^{3+D_T}(1-\beta)^{3+D_T} \tag{13}$$

Similarly, the maximum pore size $\bar{\lambda}_{\max}$ for the rough models will change correspondingly to the maximum pore size $\lambda_{\max}$ for the smooth model.

$$\bar{\lambda}_{\max} = \lambda_{\max} - 2\bar{h}_{\lambda_{\max}} \tag{14}$$

And according to the assumption of self-similarity for all pores in open-cell metal foam, $\beta = 2\bar{h}_\lambda/\lambda$ is the same in different pore sizes. Therefore, the roughness of each pore is equal.

$$\frac{2\bar{h}_\lambda}{\lambda} = \frac{2\bar{h}_{\lambda_{\max}}}{\lambda_{\max}} \tag{15}$$

According to Eqs. (13)–(15), permeability of porous media with rough surface can be expressed as:

$$K_R = \frac{\pi}{128}\frac{{L_0}^{1-D_T}}{A}\frac{D_f}{3 - D_f + D_T}\lambda_{\max}^{3+D_T}(1-\beta)^{6+2D_T} \tag{16}$$

When the surface of open-cell metal foam is smooth (i.e. $\beta = 0$), Eq. (16) can be degraded into a calculation expression for the permeability of porous media with smooth surface.

$$K = \frac{\pi}{128}\frac{{L_0}^{1-D_T}}{A}\frac{D_{f,3}}{3 - D_{f,3} + D_T}\lambda_{\max}^{3+D_T} \tag{17}$$

Under this sense, Eq. (17) has the same expression to that developed by Yu and Cheng [29] for porous media with non-rough surfaces. The model is shown to predict the permeability of mono-dispersed and bi-dispersed porous media. Here, to functionally relate the permeability for non-rough porous media with rough ones, an index is introduced as

$$\kappa = \frac{K_R}{K} = (1-\beta)^{6+2D_T} \tag{18}$$

where K_R and K demonstrate the permeability of rough and non-rough porous media, in respective. Eq. (18) indicates that the permeability of open-cell foam with rough surfaces is sensitive to surface roughness. And the permeability of porous media with rough (K_R) and smooth

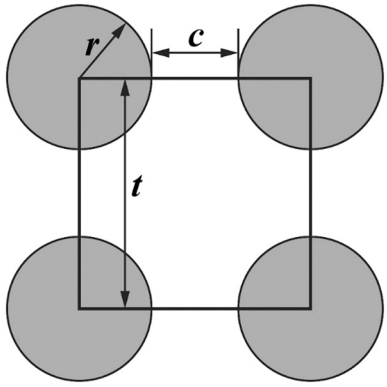

Fig. 4. Schematic diagram of micro-rods distribution.

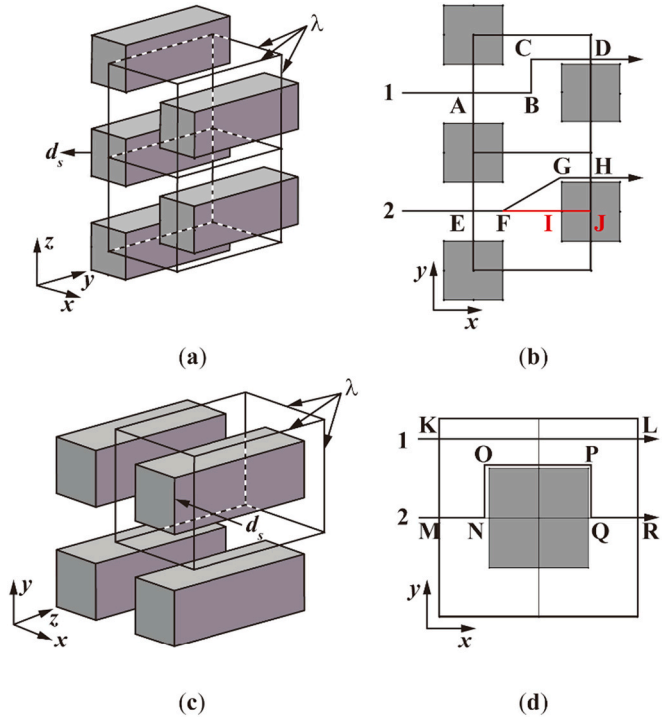

Fig. 5. Distribution of streamlines: (a) square ligaments in a dislocated and equidistant arrangement; (b) side view of streamlines flowing around square ligaments in a dislocated and equidistant arrangement; (c) square ligament in a square arrangement; (d) side view of streamlines flowing around square ligaments in a square arrangement.

surfaces (K) follow a power law.

2.2.2. Roughness

Considering that the flow resistance is mainly caused by the fluid-solid contact area. Therefore, assuming that the ratio of the equivalent average rough particle height to the average pore diameter and the actual average rough particle height to the actual average pore diameter ratio are related to the fluid-solid contact area, the relationship is expressed as:

$$\frac{\overline{h}_{\lambda_{av}}}{\lambda_{av}} = \frac{\overline{h}}{\lambda}\sqrt{\frac{S_{smooth}+S_{rough}}{S_{smooth}}} = \frac{\overline{h}}{\lambda}\sqrt{1+\frac{S_{rough}}{S_{smooth}}} \tag{19}$$

where S_{smooth} represents the total superficial area within an RS without micro-roughness, $S_{roughness}$ denotes the increased surface area by micro-rods. The increased surface area can be determined by

$$S_{rough} = 2\pi hr\varpi S_{smooth} \tag{20}$$

where ω is the number of micro-rods per unit area, h represents the height of micro-rods and r indicates the radius of micro-rods. According to Eqs. (19) and (20), the ratio of the equivalent average rough particle height to the average pore diameter can be expressed as:

$$\frac{\overline{h}_{\lambda_{av}}}{\lambda_{av}} = \frac{\overline{h}}{\lambda}\sqrt{1+2\pi hr\omega} \tag{21}$$

In the current study, two micro-rods distributions on the surface of the representative structure are considered (as shown in Fig. 4). As seen, the number of micro-rods per unit area can be obtained by:

$$\omega = \frac{1}{t^2} = \frac{1}{(2r+c)^2} \tag{22}$$

where t represents the distance between micro-rods and c is the surface distance between the two micro-rods in Fig. 4. Combining Eqs. (21) and (22), the relationship between roughness and micro-rods can be obtained as:

$$\frac{\overline{h}_{\lambda_{av}}}{\lambda_{av}} = \frac{\overline{h}}{\lambda}\sqrt{1+2\pi\frac{h}{r(2+\xi)^2}} \tag{23}$$

where $\xi = c/r$.

2.2.3. Characteristic length L_0

The characteristic length L_0 characterizes a size scale in which all the fractal pores are contained from smallest to the largest size. Within the length scale, the porosity of the foam with length L_0 can be calculated as:

$$\varepsilon = \frac{V_{pore}}{L_0^3} \tag{24}$$

where V_{pore} is the volume of all the pores in the foam. For a high porosity open-cell metallic foam, the shape of pores actually exhibits a close nature to tetradecahedral [49,50]. To simplify the current calculation, the pores are idealized as spherical ones. In a RS with side length L_0, the total pore volume may thence be calculated as [51,52]:

$$V_{pore} = \frac{\pi D_{f,3}\overline{\lambda}_{\max}^3}{6(3-D_{f,3})}(1-\varepsilon) \tag{25}$$

where $D_{f,3} = 3 - \frac{\ln\varepsilon}{\ln(\lambda_{\min}/\lambda_{\max})}$. According to Eqs. (14), (24), and (25), the characteristic length L_0 can be obtained as:

$$L_0 = \lambda_{\max}(1-\beta)\left[\frac{\pi D_{f,3}}{6(3-D_{f,3})}\frac{1-\varepsilon}{\varepsilon}\right]^{\frac{1}{3}} \tag{26}$$

2.2.4. Fractal dimension of the average tortuosity, D_T

The tortuosity is a key parameter in fractal dimension of the average tortuosity. The tortuosity of porous media is usually defined as [53]:

$$\tau = L_t/L_0 \tag{27}$$

The hydraulic diameter of open-cell metal foam with rough surface has changed thanks mainly to the existence of micro roughness. Therefore, the tortuosity of porous media with rough surface can be obtained as:

$$\tau = \frac{L_t\left(\lambda-2\overline{h}_\lambda\right)}{L_0} = \frac{\lambda^{1-D_T}\left(1-2\overline{h}_\lambda/\lambda\right)^{1-D_T}L_0^{D_T}}{L_0} = \left[\frac{\lambda}{L_0}\left(1-\frac{2\overline{h}_\lambda}{\lambda}\right)\right]^{1-D_T} \tag{28}$$

Taking the natural logarithm for both sides of Eq. (28), the tortuous fractal dimension can be expressed as:

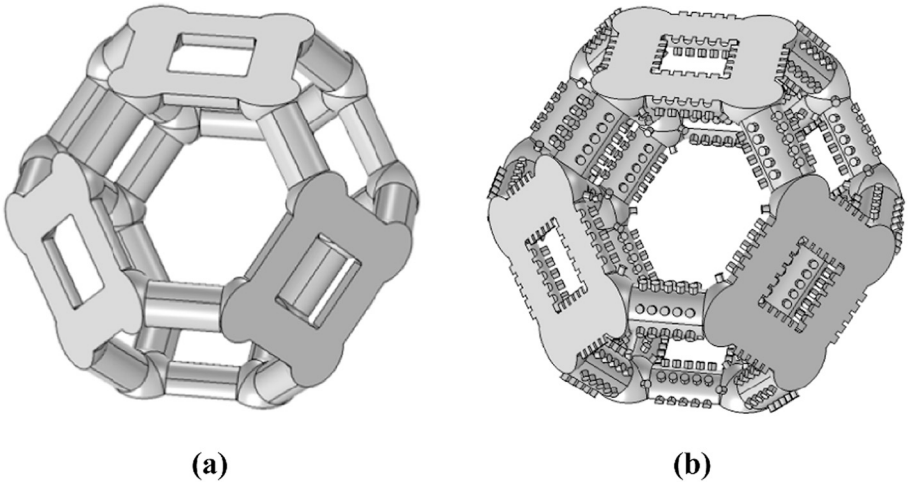

Fig. 6. Tetradecahedral unit cell: (a) smooth surface; (b) rough surface.

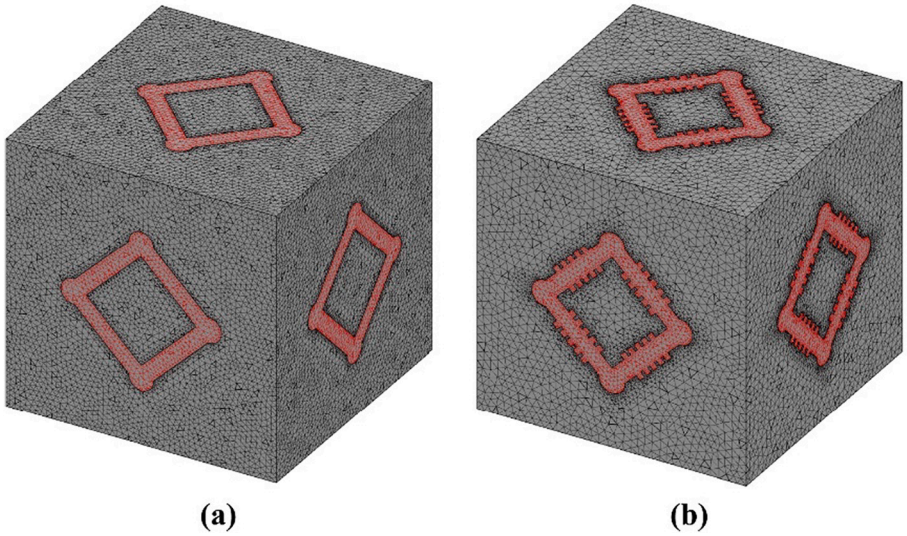

Fig. 7. Representative mesh: (a) smooth surface; (b) rough surface.

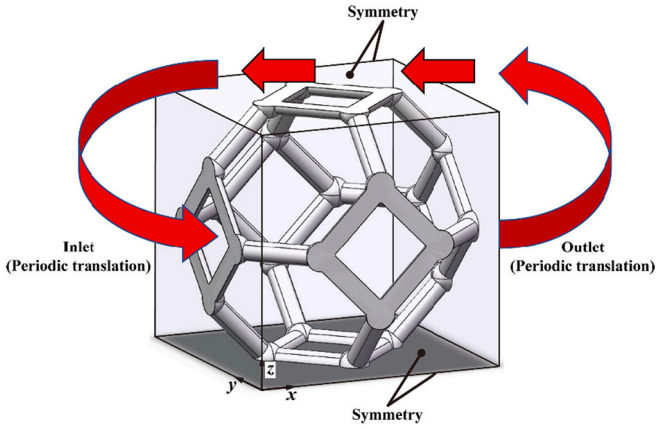

Fig. 8. Schematic diagram of boundary conditions.

Table 1
Mesh independence verification.

Foam sample	Mesh 1	Mesh 2	Mesh 3
	277060	1650528	2666312
		ΔP (Pa)	
Smooth-Foam1	3.00×10^{-3}	3.08×10^{-3}	3.09×10^{-3}

$$D_T = 1 + \frac{ln\tau}{ln\left[\frac{L_0}{\lambda\left(1-2\bar{h}_\lambda/\lambda\right)}\right]} \tag{29}$$

Through the manipulation on the replacement of the tortuosity τ and the pore diameter λ in Eq. (29) by the average tortuosity τ_{av} and the average pore diameter λ_{av}, the analytical expression for the average tortuosity fractal dimension of porous media within rough surface is therefore:

Table 2
Validation of fractal analytical model of open-cell metal foam with rough surface [27,28].

Foam sample	ε	λ (mm)	r (μm)	h (μm)	r (mm)	K (exp) (m^2)	K (pre) (m^2)	RD (%)
ZnO micro-rods	0.92	1	2.5	30	0.12	7.98	7.99	0.13
Co_3O_4 (2 h)	0.92	2.5	2.5	30	0.11	8.71	8.82	1.25
Co_3O_4 (6 h)	0.92	2.5	2.5	40	0.12	7.00	6.61	5.90
Co_3O_4 (10*h*)	0.92	2.5	2.5	50	0.13	5.52	5.83	5.32

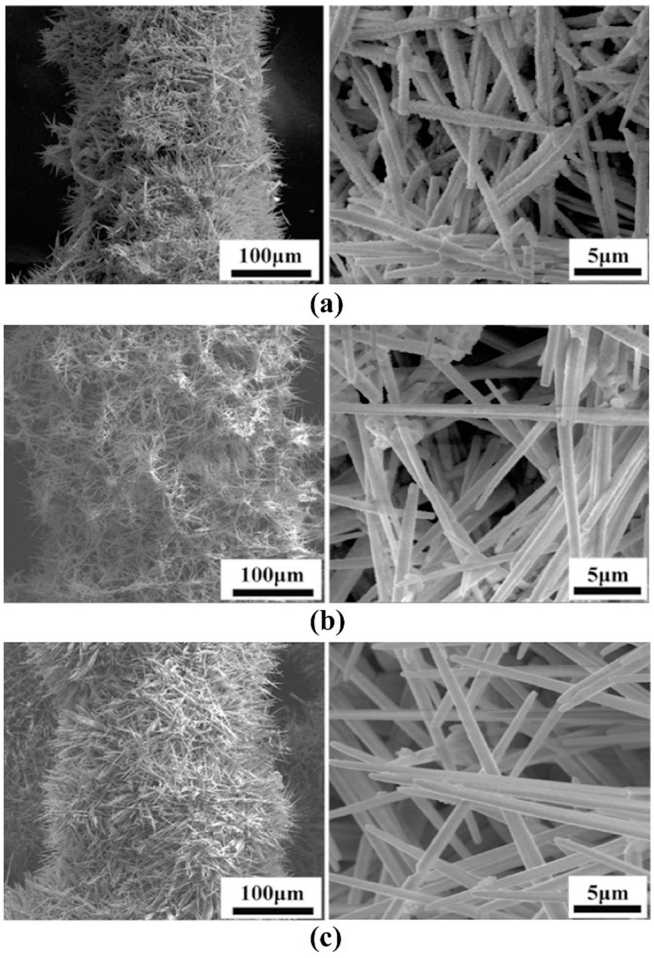

Fig. 9. The height of micro-rods on the surface of open-cell metal foam ligament varies under different growth times [28]: (a) 2 h; (b) 6 h; (c) 10 h.

$$D_T = 1 + \frac{ln\tau_{av}}{ln\left[\frac{L_0}{\lambda_{av}\left(1-2\overline{h}_{\lambda_{av}}/\lambda_{av}\right)}\right]} \tag{30}$$

Due to the similarity of porous fractal pores, the equation of $\overline{h}_{\lambda}/\lambda = \overline{h}_{\lambda_{av}}/\lambda_{av}$ is satisfied. With $\overline{h}_{\lambda_{av}}/\lambda_{av} = 0$, the average tortuosity of porous media with smooth surface can be expressed as:

$$D_T = 1 + \frac{ln\tau_{av}}{ln(L_0/\lambda_{av})} \tag{31}$$

where λ_{av} and τ_{av} are the average pore diameter and the average tortuosity, respectively. Here, $D_T = 1$ represents a straight channel/tube, and $D_T = 3$ represents a tortuous channel/tube filling a three-dimensional space. For a three-dimensional porous medium, $1 < D_T < 3$.

Using fractal theory, the average pore diameter of the foam is given as [54]:

Table 3
Tetradecahedral geometric parameters and simulation results.

Foam sample	ε	λ (mm)	t_s (mm)	R (mm)	h (mm)	r_s (mm)	K/t_s^2 (Sim)
Smooth-Foam1	0.814	2.5	0.22	0.33	N/A	N/A	0.243
Smooth-Foam2	0.845	2.5	0.2	0.3	N/A	N/A	0.350
Smooth-Foam3	0.873	2.5	0.18	0.27	N/A	N/A	0.509
Smooth-Foam4	0.899	2.5	0.16	0.24	N/A	N/A	0.759
Smooth-Foam5	0.922	2.5	0.14	0.21	N/A	N/A	1.161
Smooth-Foam6	0.942	2.5	0.12	0.18	N/A	N/A	1.856
Smooth-Foam7	0.960	2.5	0.1	0.15	N/A	N/A	3.116
Smooth-Foam8	0.974	2.5	0.08	0.12	N/A	N/A	5.754
Smooth-Foam9	0.979	2.5	0.072	0.108	N/A	N/A	7.572
Rough-Foam1	0.809	2.5	0.22	0.33	0.05	0.03	0.211
Rough-Foam2	0.839	2.5	0.2	0.3	0.05	0.03	0.295
Rough-Foam3	0.867	2.5	0.18	0.27	0.05	0.03	0.427
Rough-Foam4	0.891	2.5	0.16	0.24	0.05	0.03	0.619
Rough-Foam5	0.914	2.5	0.14	0.21	0.05	0.03	0.933
Rough-Foam6	0.935	2.5	0.12	0.18	0.05	0.03	1.471
Rough-Foam7	0.952	2.5	0.1	0.15	0.05	0.03	2.448
Rough-Foam8	0.967	2.5	0.08	0.12	0.05	0.03	4.413
Rough-Foam9	0.971	2.5	0.072	0.108	0.05	0.03	5.784

$$\lambda_{av} = \frac{D_{f,3}\lambda_{\min}}{D_{f,3} - 1} \tag{32}$$

When $D_{f,3}$ and L_0 are determined, the only key parameter that needs to be characterized is the average tortuosity τ_{av}. The tortuosity of a porous medium is defined as the ratio of the length for a real tortuous flow path to that of a straight (minimal) one [53,55], accounting for the elongation extent of the flow path. Since there are numerous streamlines in porous medium, it had been demonstrated that the average of representative streamlines could be used to estimate the average tortuosity [56]. The distribution of streamlines in the cubic *RS* is depicted in Fig. 5. Since the pore sizes and distributions of open-cell metal foams are random, it is impossible to consider every streamline distribution by theoretical calculations. To address this issue and find solution to the calculation on average tortuosity, two representative structures of ligaments distribution are selected, as shown in Fig. 5(a) and (c). One distribution of ligaments is the dislocated and equidistant arrangement in Fig. 5(a), and the other is the square arrangement in Fig. 5(c). To further simplify the calculation, the irregular pore structures are simplified into cubic representative structures.

For open-cell metal foams with idealized pore structures, the average

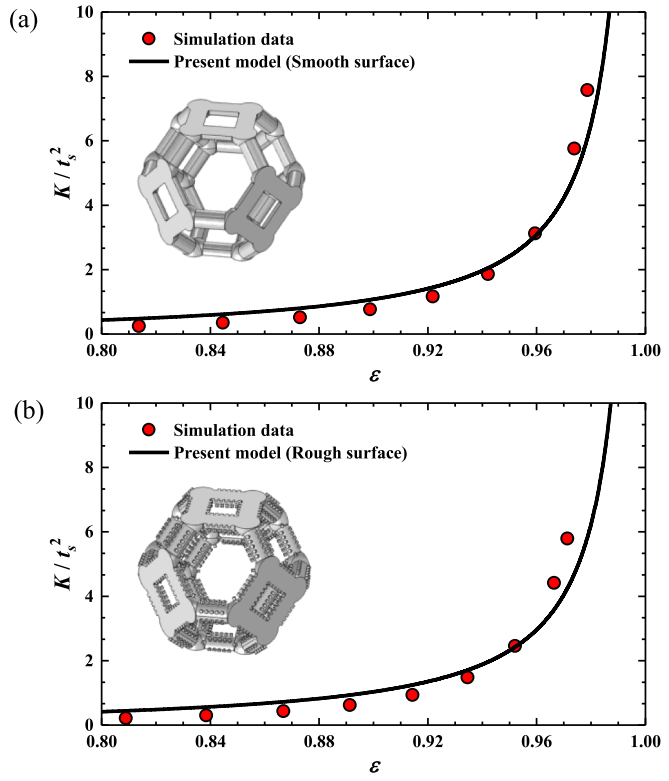

Fig. 10. Comparison of theoretical prediction and numerical simulation: (a) smooth surface; (b) rough surface.

tortuosity is determined by using a weighted average over all possible streamlines around two representative ligament arrangements in Fig. 5 (b) and (d), as:

$$\tau_{av} = \sum_{i=1}^{n} a_i \tau_i \tag{33}$$

where n is the total number of possible streamlines, a represents the weight value ($\sum_{i=1}^{n} a_i = 1$), and τ_i denotes the tortuosity of the i-th flow streamline. When $a_1 = a_2 = \cdots = a_n$, Eq. (33) is reduced to a simple statistical average [56]. Considering that there are countless flow paths exist in a *RS*, it seems impossible to directly calculate all path lines of fluid flow to determine the average tortuosity. It was suggested that the average tortuosity is related to the averaged tortuosity for two representative flow paths: the longest and the shortest paths [56]. The length, width and height for the representative structure (*RS*) are denoted by λ in Fig. 5(a) and (c). The total pore volume in the *RS* can be calculated by:

$$V_{RS-pore} = \lambda^3 - \lambda \cdot d_s^2 \tag{34}$$

where d_s is the side length of the square ligament. Then, for the structures of Fig. 5(a) and (c), the porosity can be calculated by:

$$\varepsilon = \frac{V_{RS-pore}}{V_{RS-total}} = 1 - \left(\frac{d_s}{\lambda}\right)^2 \tag{35}$$

where the total volume of the cubic representative structure is $V_{RS-total} = \lambda^3$. It follows that:

$$\frac{d_s}{\lambda} = \sqrt{1-\varepsilon} \tag{36}$$

For streamline 1 in Fig. 5(b), $l_{AB} = l_{CD} = \lambda/2$ and $l_{BC} = d_s/2$. The tortuosity can thence be calculated as:

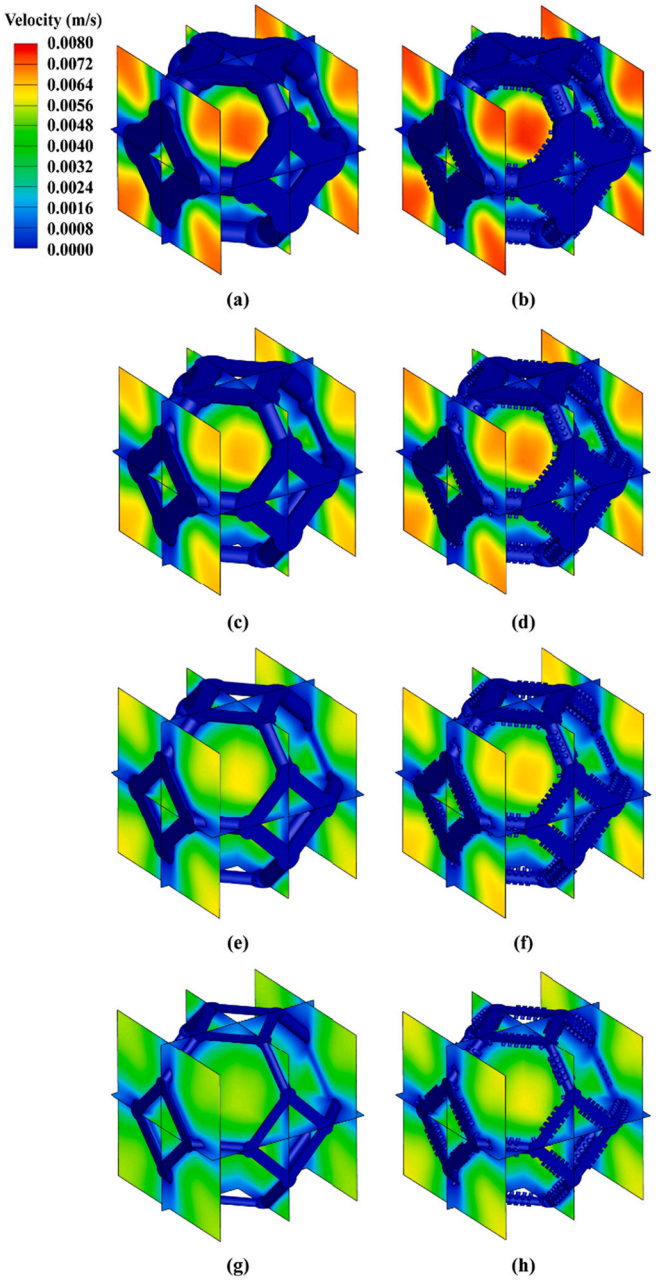

Fig. 11. Velocity distribution with different porosities: (a) Smooth-Foam2; (b) Rough-Foam2; (c) Smooth-Foam4; (d) Rough-Foam4; (e) Smooth-Foam6; (f) Rough-Foam6; (g) Smooth-Foam8; (h) Rough-Foam8.

$$\tau_{1-1} = \frac{l_{AB} + l_{BC} + l_{CD}}{l_{AB} + l_{CD}} = 1 + \frac{1}{2}\frac{d_s}{\lambda} = 1 + \frac{\sqrt{1-\varepsilon}}{2} \tag{37}$$

Similarly, for streamline 2 in Fig. 5(b), as $l_{EF} = l_{GH} = l_{IJ} = l_{GI} = d_s/2$, $l_{FI} = \lambda - d_s$ and $l_{FG} = \sqrt{l_{GI}^2 + l_{FI}^2} = \sqrt{\left(\frac{d_s}{2}\right)^2 + (\lambda - d_s)^2}$, the tortuosity is determined by:

$$\tau_{1-2} = \frac{l_{EF} + l_{FG} + l_{GH}}{l_{EF} + l_{FI} + l_{IJ}} = \frac{d_s + \sqrt{\left(\frac{d_s}{2}\right)^2 + (\lambda - d_s)^2}}{d} = \sqrt{1-\varepsilon} + \frac{1}{2}\sqrt{9 - 5\varepsilon - 8\sqrt{1-\varepsilon}} \tag{38}$$

For the distribution of ligaments depicted in Fig. 5(b), the

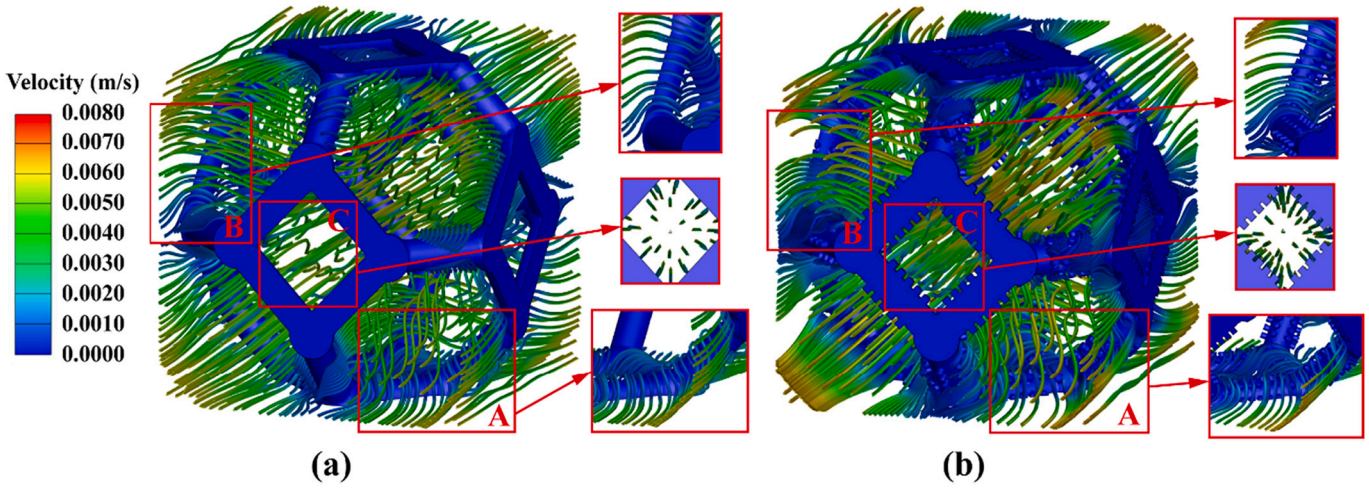

Fig. 12. Schematic diagram of the streamline: (a) Smooth-Foam6; (b) Rough-Foam6.

distribution proportion of streamlines 1 and 2 is not affected by the porosity. Therefore, streamlines 1 and 2 in Fig. 5(b) have identical weight, e.g., $a_{1-1} = a_{1-2}$ and $a_{1-1} + a_{1-2} = 1$. The tortuosity is then calculated by a simple weighted average, as:

$$\tau_1 = a_{1-1}\tau_{1-1} + a_{1-2}\tau_{1-2} = \frac{1}{2}\tau_{1-1} + \frac{1}{2}\tau_{1-2} = \frac{2 + 3\sqrt{1-\varepsilon} + \sqrt{9 - 5\varepsilon - 8\sqrt{1-\varepsilon}}}{4} \tag{39}$$

where a_{1-1} and a_{1-2} are separately the weight values of streamline 1 and 2 in Fig. 5(b).

For streamline 1 in Fig. 5(d), its actual length l_{GH} and the straight length of flow l_{GH} are equal in the cell, yielding:

$$\tau_{2-1} = \frac{l_{GH}}{l_{GH}} = 1 \tag{40}$$

For streamline 2 in Fig. 5(d), the streamline of the ligament boundary layer is considered to fit the ligament surface because of the thin boundary thickness of the ligament surface. Since $l_{MN} = l_{QR} = \frac{\lambda}{2}$, $l_{NO} = l_{PQ} = \frac{d_s}{2}$ and $l_{OP} = d_s$, the tortuosity can be calculated, as:

$$\tau_{2-2} = \frac{l_{MN} + l_{NO} + l_{OP} + l_{PQ} + l_{QR}}{l_{MN} + l_{OP} + l_{QR}} = \frac{\lambda + d_s}{\lambda} = 1 + \sqrt{1-\varepsilon} \tag{41}$$

As the volume of the ligament increases, the proportion of straight streamline decreases while the proportion of tortuous streamline increases. Therefore, the streamlines 1 and 2 in Fig. 5(d) are related to the volume of the ligaments in the unit. The two weights of streamlines in Fig. 5(d) are $a_{2-1} = \frac{\lambda^3 - \lambda d_s^2}{\lambda^3}$ and $a_{2-2} = \frac{\lambda {d_s}^2}{\lambda^3}$, yielding:

$$\tau_2 = a_{2-1}\tau_{2-1} + a_{2-2}\tau_{2-2} = \left(\frac{\lambda^3 - \lambda d_s^2}{\lambda^3}\right)\tau_{2-1} + \frac{\lambda {d_s}^2}{\lambda^3}\tau_{2-2} = 1 + (1-\varepsilon)\sqrt{1-\varepsilon} \tag{42}$$

Generally, the pores are randomly distributed and the pore sizes are different in high-porosity open-cell metal foams. Consequently, proportions of the two ligament distributions in Fig. 5(a) and (c) cannot be directly measured. In the current study, it is assumed that the two distributions have the same probability, i.e., $a_1 = a_2 = \frac{1}{2}$. Here, a_1 and a_2 are the weight values for the dislocated and equidistant arrangement of Fig. 5(a) and the weight value for the square arrangement of Fig. 5(c), in respective. According to Eqs. (39) and (42), the average tortuosity can be finalized as:

$$\tau_{av} = a_1\tau_1 + a_2\tau_2 = \frac{1}{2}\tau_1 + \frac{1}{2}\tau_2 = \frac{6 + (7-4\varepsilon)\sqrt{1-\varepsilon} + \sqrt{9 - 5\varepsilon - 8\sqrt{1-\varepsilon}}}{8} \tag{43}$$

Finally, the fractal dimension of average tortuosity is obtained by Eqs. (26), (30), (32), and (43).

$$D_T = 1 + \frac{ln\left\{\frac{1}{8}\left[6 + (7-4\varepsilon)\sqrt{1-\varepsilon} + \sqrt{9 - 5\varepsilon - 8\sqrt{1-\varepsilon}}\right]\right\}}{ln\left\{\frac{\lambda_{\max}}{\lambda_{\min}}^{\frac{D_{f,3}-1}{D_{f,3}}}\left[\frac{\pi D_{f,3}}{6\left(3-D_{f,3}\right)}\frac{1-\varepsilon}{\varepsilon}\right]^{\frac{1}{3}}\right\}} \tag{44}$$

2.2.5. Maximum pore diameter

In the current fractal model development, since the self-similarity of pores, the maximum pore corresponds to the maximum size of a pore. In the *RS* shown in Fig. 2, the maximum pore diameter can be calculated from the maximum pore volume $V_{\max-pore}$ as:

$$\lambda_{\max} = \sqrt[3]{V_{max-pore}} = \sqrt[3]{V_{total-pore} - V_{solid-pore}} = \sqrt[3]{V_{solid-pore}\varepsilon/(1-\varepsilon)} \tag{45}$$

where $V_{solid-pore}$ and $V_{total-pore}$ are the volume of solid ligaments and the total volume of pores within the *RS*, in respective. The analytical expression that is used to calculate the total solid volume of the *RS* in Fig. 2 is

$$V_{solid} = t_s^3\left[\frac{3\pi}{\gamma} - \frac{8}{3}\pi k^3 + 4\pi\left(k^2-1\right)\sqrt{k^2-1}\right] \tag{46}$$

where $k = R/t_s$, $\gamma = t_s/d$, R is the radius of the connected nodes, d demonstrates the pore size and t_s represents the thickness of ligament. According to the definition of porosity, the porosity of the cubic unit cell with nodes in Fig. 2 can be obtained as:

$$\varepsilon = \frac{V_{total-pore} - V_{solid-pore}}{V_{total-pore}} = 1 - \gamma^3\left[\frac{3\pi}{\gamma} - \frac{8}{3}\pi k^3 + 4\pi\left(k^2-1\right)\sqrt{k^2-1}\right] \tag{47}$$

where $V_{total-pore} = d^3$ is the total volume for a *RS*.

2.2.6. Permeability formula

Eventually, by determining all the above key parameters, the analytical formulas for the permeability of open-cell metallic foam with rough surfaces can be obtained as:

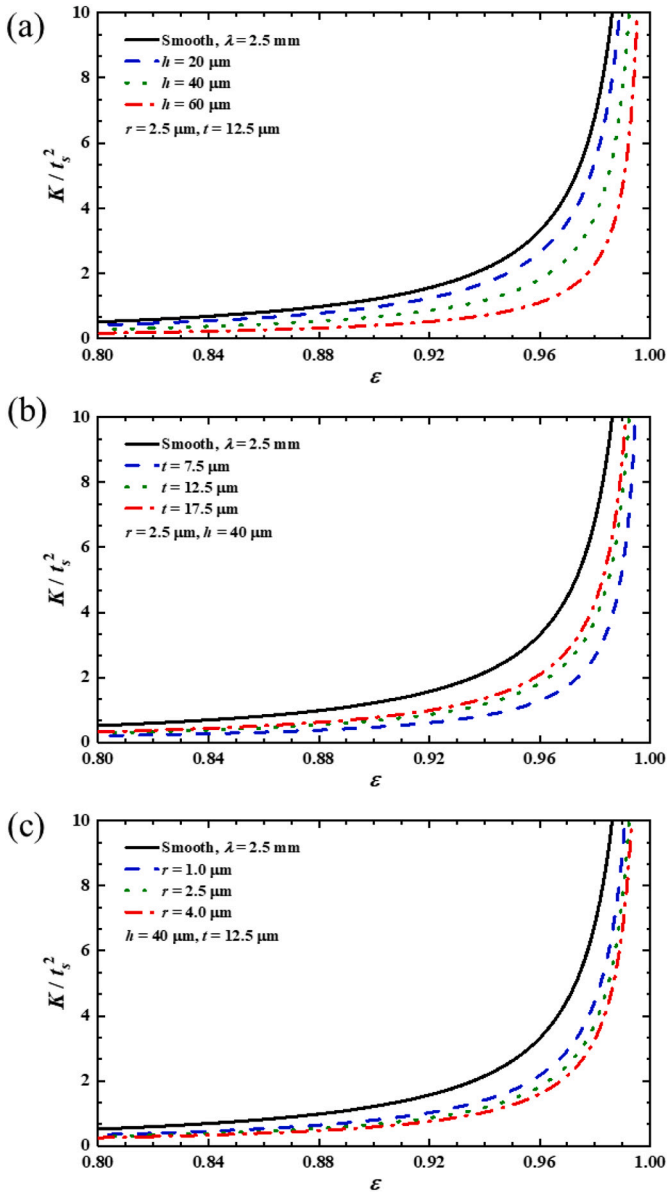

Fig. 13. Relationship between porosity and open-cell metal foam with the rough surfaces: (a) effect of micro-rods height; (b) effect of micro-rods interval; (c) effect of micro-rods radius.

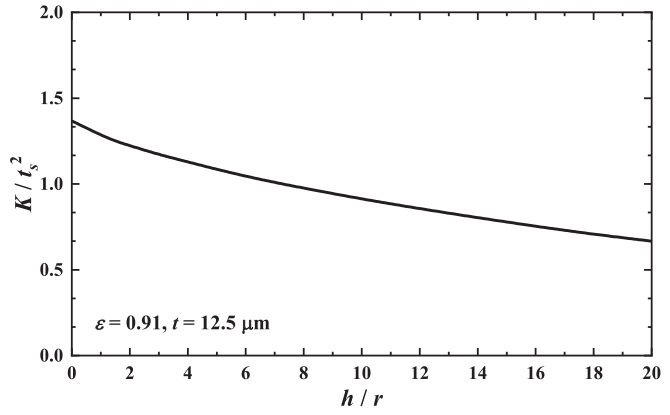

Fig. 14. Permeability dependence on the micro-rod height-to-radius ratio.

$$\frac{K_R}{t_s^2}=\frac{\pi}{128}\frac{D_{f,3}}{3-D_{f,3}+D_T}\left[\frac{\pi D_{f,3}}{6(3-D_{f,3})}\frac{1-\varepsilon}{\varepsilon}\right]^{-\frac{1+D_T}{3}}\left\{\left[\frac{3}{\gamma}-\frac{8}{3}k^3+4\left(k^2-1\right)\sqrt{k^2-1}\right]\frac{\pi\varepsilon}{1-\varepsilon}\right\}^{\frac{2}{3}}(1-\beta)^{5+D_T} \tag{48}$$

where the fractal dimension of pore size distribution $D_{f,3}$ is calculated by Eq. (7), the roughness β is obtained by Eq. (21), and the fractal dimension D_T is predicted by Eq. (44). It is important to note that, unlike previous permeability models, the current permeability model (Eq. (49)) does not contain any empirical or curve-fitting parameters.

3. Pore-scale numerical simulation

In addition to the development of analytical models, it is of critical importance to learn the transport phenomena in open-cell metal foam at pore scale. Only through this can the effects of the local ligaments and its surface roughness on the flow behavior be understood. Fig. 6 illustrates the tetradecahedral unit cell that is used to directly simulate the permeable flow in open-cell metal foam: (a) denotes the metal foam structure without surface roughness and (b) indicates the structure with surface micro roughness. There are two main reasons why the cubic unit cell that is the same as the representative structure (*RS*) is not selected as the geometric model for direct numerical simulation. One of the reasons is that there are different size pores in the tetradecahedral unit, while six faces of cubic unit cell have the same pores (see Fig. 2). In the current study, the fractal structure of open-cell metal foam assumes that pore shapes are similar, but the size and distribution of pores are random. Therefore, a cubic unit cell cannot be selected for direct simulation of open-cell metal foam permeability. The pores of different sizes in the tetradecahedral unit could reflect the situation of different pore sizes. Another reason is that the existing literature [57] demonstrates that the real pore structure of open-cell metal foam is closer to tetradecahedron. Therefore, the tetradecahedral unit cell is selected to simulate the permeability of open-cell metal foam at pore scale. In this way, a more accurate numerical simulation results of the permeability of open-cell metal foam can be obtained.

The ANSYS ICEM CFD software is used for meshing and the unstructured tetrahedral meshes with the fluid-solid contact surface appropriately densified are generated, as shown in Fig. 7. The boundary conditions are set in Fig. 8: the inlet and outlet are set to periodic translation boundary conditions with a mass flow rate of 2.37×10^{-8} kg · s^{-1}; the remaining four faces are symmetrical boundary conditions. The Reynolds number is always less than 1, so that the influence of fluid inertial force can be ignored. The fluid is air whose density is 1.185 kg · m^{-3} and the viscosity coefficient is 1.82×10^{-5} kg · m^{-1} · s^{-1}. The commercial software ANSYS-CFX 19.1 is used for direct numerical simulations to explore the transport properties of open-cell metal foam with rough surfaces. The convergence residuals for continuity and momentum equations in the each iteration are set to be 10^{-7}, to ensure the accuracy of the calculation.

Three different numbers of meshes are generated to verify the mesh independence, and the results are shown in Table 1. It can be found that the calculation results of pressure drop remain unchanged when the number of mesh elements is larger than 1.65 million. Therefore, 1,650,528 tetrahedron elements are selected for numerical simulation.

4. Results and discussion

4.1. Model verification

To verify the validity of the fractal analytical permeability model for open-cell metal foam with rough surfaces, the analytical prediction and experimental results are compared (as shown in Table 2). Table 2 summarizes the detailed sample geometric parameters, the comparison

between the model prediction and experimental results, and the analysis of the relative deviations. For quantitative comparison, relative deviation (*RD*) is applied to evaluate different permeability models, which is defined by:

$$RD = \left| \frac{K_{\text{pre}} - K_{\text{exp}}}{K_{\text{exp}}} \right| \tag{49}$$

where the subscripts "exp" and "pre" denote separately the experimental measurement and model prediction.

The porosity of all four samples is 0.92 in Table 2, with pore sizes of 1.0 mm and 2.5 mm before the ligament surfaces of open-cell metal foam are covered with rough micro-rods. The micro-rods can be divided into two types: one is ZnO micro-rods and the other is Co_3O_4 micro-rods. The radius and height of ZnO micro-rods are 2.5 μm and 30 μm [27], respectively. The radius of Co_3O_4 micro-rods is 2.5 μm, and the height of Co_3O_4 micro-rods changes with the processing time [28]. When the processing time ranges from 2 to 10 h, the height of micro-rods varies from 30 to 50 μm [28], as shown in Fig. 9.

As noticed in Table 2, the fractal analytical model can predict the permeability of open-cell metal foam with rough surface well, and the relative deviation (*RD*) between theoretical predictions and experimental results is within 6%. Besides, the permeability in the Co_3O_4 samples decreases significantly with the increase in the height of the micro-rods. This indicates that the micro-rods height plays a vital role in affecting the permeability of open-cell foam.

4.2. Numerical simulation results

To further verify the applicability of the theory and learn the transport physics at pore scale, theoretical predictions are compared with direct numerical simulation of the tetradecahedral unit.

Table 3 shows the geometric parameters of the tetradecahedral unit and the corresponding simulation results. There are totally eighteen geometric models with and without micro-rods as surface roughness. As seen in Table 3, the appearance of micro-rods notably reduces the porosity and permeability of the original smooth tetradecahedral unit cell. To show the relationship between theoretical predictions and simulation results, Fig. 10 illustrates the comparison between theoretical predictions and simulation results for smooth and rough surfaces in Fig. 10 (a) and (b), respectively. It can be noticed that there is a good agreement between the two approaches, further indicating the applicability of the established analytical model.

Fig. 11 depicts the velocity distribution in the tetradecahedral unit cell with smooth and rough surfaces under different porosities. Fig. 11 (a), (c), (e) and (g) demonstrate the velocity distribution in the cells with smooth surfaces, and Fig. 11(b), (d), (f) and (h) show the one in the roughed cells, denoting Foam 2, 4, 6, and 8, in respective. With the numbers for Foam in Fig. 11 increases, i.e. Foam 2, Foam 4, and Foam 6, their ligament thickness and node radius gradually decrease, and thus their porosity gradually increases. The flow velocity in the pore center area decreases with the increase in porosity, as depicted the red spots in Fig. 11. The inlet and outlet of the tetradecahedral unit cell are set to the periodic translational boundary with constant mass flow. The higher the porosity is, the larger the window area is resulted in, and the smaller the velocity will be (the smaller red spots in Fig. 11). Therefore, the flow velocity in the center of pore decreases as the porosity increases.

For the same ligament thickness and node radius, such as Fig. 11(a) and (b), (or other group of (c) and (d), (e) and (f), (g) and (h)), it can be found that the velocity at pore center area with rough surface is higher than that with smooth surface. Macroscopically, micro-rods reduces the porosity of the original smooth tetradecahedral unit cell. The flow velocity in the center of pore therefore increases under the constant mass flow rate. To reveal the specific microscopic mechanism that micro-rods affect the permeability of tetradecahedral unit cell, the streamlines of sample Foam6 is analyzed in Fig. 12 separately for (a) of smooth surfaces and (b) of rough surfaces. As seen, the two tetradecahedral unit cell have the same ligament thickness and node radius. It is found that the tortuosity of streamlines near the micro-rods increases significantly, and the flow velocity of streamlines near the rods decreases by comparing the areas A and B in Fig. 12(a) and (b). In Fig. 12(a), the main factors impeding fluid motion are the ligaments and nodes of the unit cell. However, the micro-rods further impede the fluid motion in Fig. 12(b). This is reflected in Fig. 11 where the micro-rods increase the slow-flowing area near the ligaments and nodes. For the central region C in Fig. 12, the micro-rods have almost influence upon the streamlines. Due to the constant mass flow, the micro-rods cause the slow flow region to increase near the ligaments and nodes, and the relative increase in the velocity of the pore center area when the ligament thickness and node radius of the two unit cells are the same. In addition to increasing the tortuosity of the fluid passing through the ligaments and nodes, the micro-rods also increase the contact surface area between the fluid and the solid in the tetradecahedral unit cell. The viscous flow resistance is therefore increased. Via these factors is the permeability of the unit cell with micro-rods reduced, under the conditions of the same ligament thickness and node radius as the original foam cell.

4.3. Dependence of permeability on porosity

Fig. 13 illustrates the relationship between the dimensionless permeability of open-cell metal foam K/t_s^2 and the foam porosity ε under different microstructure parameters (height, interval, radius) of the micro-rods. In Fig. 13, the dimensionless permeability decreases with the increase in porosity. As $0.80 \leq \varepsilon < 0.90$, the dimensionless permeability increases slowly with porosity; when $0.90 \leq \varepsilon < 1.0$, a rapid increment is found for the permeability as a function of porosity. This can be understood as follows: the porosity increases and the proportion of solid phase of open-cell metal foam decreases. As porosity approaching to unit, the permeability is close to the limit (infinity). The flow resistance decreases and the permeability increases.

In Fig. 13, it can be seen that open-cell metal foam with smooth surface has the largest permeability under the same porosity than the other foams with rough surfaces. Micro-rods on the surface of metal foam ligament increase the flow resistance and cause the permeability to decrease. The radius of micro-rods is 2.5 mm and the interval of micro-rods is 12.5 mm in Fig. 13(a). In Fig. 13(a), as the height of micro-rods increases from 20 μm to 60 μm, the permeability gradually decreases. This is due mainly to the increment in the height of micro-rods which leads to an enlarged surface area of open-cell metal foam (i.e., the more contact and interactions between in fluid and solid ligaments). Consequently, the flow resistance of the fluid through the metal foam increases and thus the permeability decreases. In Fig. 13(b), the radius and height of the micro-rod are 2.5 μm and 40 μm, and the interval of micro-rods increases from 7.5 μm to 17.5 μm. The increase in the distance between micro-rods is equivalent to the decrease in the number of micro-rods per unit area, and the roughness of the ligament surface decreases. The flow resistance of the fluid through the metal foam decreases, and the permeability increases. In Fig. 13(c), the height and interval of the micro-rods are 40 μm and 12.5 μm, respectively. And the radius of micro-rods varies from 1 μm to 4 μm. With the porosity fixed, the larger the radius of micro-rods, the lower the permeability is resulted in. This is thanks mainly to the fact that under the same interval, the number of micro-rods per unit area remains unchanged. The total surface area of micro-rods changes to a larger value as a bigger radius of micro-rods. Therefore, the flow resistance increases (larger surface area) and the permeability decreases.

4.4. Effect of micro-rod height-to-radius ratio

Fig. 14 depicts the relationship between the dimensionless permeability and the height-to-radius ratio. The porosity for metal foam is 0.91 and a pore size is 2.5 mm. For the rough elements, the interval between

micro-rods is 12.5 μm. To discuss the effect of the micro-rods high-to-radius ratio on the foam permeability, it is assumed that the volume of the micro-rods remains constant. In this way, the number of micro-rods per unit area and the total volume also remain unchanged. When the volume of the micro-rods keeps constant, the different height-to-radius ratios will change the shape of the micro-rods. As increasing the height-to-radius ratio, the micro-rod varies to be a long and thin cylinder. When the height-to-radius decreases, the micro-rod thus looks like a short and thick one. It can be obtained in Fig. 14 that the dimensionless permeability decreases with the increase in the height-to-radius ratio. As the height-to-radius increases, the surface of ligaments becomes rougher, which leads to decrement in permeability. When the height-to-radius ratio is reduced, the surfaces of ligaments becomes more smoother, causing to improvement in permeability.

5. Conclusion

Based on the fractal theory for describing metal foam with surface roughness, a permeability model for metal foam with rough surfaces is developed. Permeability varies functionally with pore parameters (porosity ε, pore size λ), micro-rods geometry, and a series of fractal dimensions. The model predictions are in good agreement with experimental results, which verifies the analytical model. The tetradecahedral unit cell is used to simulate the permeable flow in open-cell metal foam. The following concluding remarks can be reached:

(1) The micro roughness on the metal foam porous surface significantly reduce the foam permeability;
(2) Non-dimensional permeability decreases as an increase in micro-rod height and radius, but increases with micro-rod interval;
(3) The pore-scale simulation confirms the fact the reduced permeability is caused mainly by the increased flow tortuosity and the surface friction between fluid transport and the micro roughness.

Declaration of Competing Interest

The authors declare that they have no known competing financial interests or personal relationships that could have appeared to influence the work reported in this paper.

Acknowledgements

This work was supported by the National Natural Science Foundation of China (51976155, 12032010), the Fundamental Research Funds for Central Universities (xtr042019019), and the Open Fund of the State Key Laboratory of Mechanics and Control of Mechanical Structures (MCMS-E0219K02, MCMS-I-0219K01). One of the authors (Xiaohu Yang) gratefully acknowledged the support of K. C. Wong Education Foundation.

References

[1] T.J. Lu, H. Stone, M. Ashby, Heat transfer in open-cell metal foams, Acta Mater. 46 (1998) 3619–3635.
[2] Z. He, L. Zhan, Q. Wang, S. Song, J. Chen, K. Zhu, et al., Increasing the activity and stability of chemi-deposited palladium catalysts on nickel foam substrate by electrochemical deposition of a middle coating of silver, Sep. Purif. Technol. 80 (2011) 526–532.
[3] D.M. Burke, M.A. Morris, J.D. Holmes, Chemical oxidation of mesoporous carbon foams for lead ion adsorption, Sep. Purif. Technol. 104 (2013) 150–159.
[4] A. Kumar, R. Reddy, Modeling of polymer electrolyte membrane fuel cell with metal foam in the flow-field of the bipolar/end plates, J. Power Sources 114 (2003) 54–62.
[5] H. Tawfik, Y. Hung, D. Mahajan, Metal bipolar plates for PEM fuel cell—a review, J. Power Sources 163 (2007) 755–767.
[6] J. Guo, Z. Liu, Z. Du, J. Yu, X. Yang, J. Yan, Effect of fin-metal foam structure on thermal energy storage: an experimental study, Renew. Energy 172 (2021) 57–70.
[7] X. Yang, X. Wang, Z. Liu, Z. Guo, L. Jin, C. Yang, Influence of aspect ratios for a tilted cavity on the melting heat transfer of phase change materials embedded in metal foam, Int. Commun. Heat Mass Transf. 122 (2021), 105127.
[8] L. Li, B. Yu, Fractal analysis of the effective thermal conductivity of biological media embedded with randomly distributed vascular trees, Int. J. Heat Mass Transf. 67 (2013) 74–80.
[9] J. Zhang, Lattice Boltzmann method for microfluidics: models and applications, Microfluid. Nanofluid. 10 (2011) 1–28.
[10] D. Mu, Z.-S. Liu, C. Huang, N. Djilali, Determination of the effective diffusion coefficient in porous media including Knudsen effects, Microfluid. Nanofluid. 4 (2008) 257–260.
[11] H.J. Keh, L.Y. Hsu, Diffusioosmotic flow of electrolyte solutions in fibrous porous media at arbitrary zeta potential and double-layer thickness, Microfluid. Nanofluid. 7 (2009) 773–781.
[12] B. Straughan, A. Harfash, Instability in Poiseuille flow in a porous medium with slip boundary conditions, Microfluid. Nanofluid. 15 (2013) 109–115.
[13] D. Shou, J. Fan, M. Mei, F. Ding, An analytical model for gas diffusion though nanoscale and microscale fibrous media, Microfluid. Nanofluid. 16 (2014) 381–389.
[14] X. Yang, T. Lu, T. Kim, A simplistic model for the tortuosity in two-phase close-celled porous media, J. Phys. D. Appl. Phys. 46 (2013), 125305.
[15] M. Lacroix, P. Nguyen, D. Schweich, C.P. Huu, S. Savin-Poncet, D. Edouard, Pressure drop measurements and modeling on SiC foams, Chem. Eng. Sci. 62 (2007) 3259–3267.
[16] K. Hooman, N. Dukhan, A theoretical model with experimental verification to predict hydrodynamics of foams, Transp. Porous Media 100 (2013) 393–406.
[17] N. Dukhan, Correlations for the pressure drop for flow through metal foam, Exp. Fluids 41 (2006) 665–672.
[18] J.-F. Despois, A. Mortensen, Permeability of open-pore microcellular materials, Acta Mater. 53 (2005) 1381–1388.
[19] P. Du Plessis, A. Montillet, J. Comiti, J. Legrand, Pressure drop prediction for flow through high porosity metallic foams, Chem. Eng. Sci. 49 (1994) 3545–3553.
[20] A. Bhattacharya, V.V. Calmidi, R.L. Mahajan, Thermophysical properties of high porosity metal foams, Int. J. Heat Mass Transf. 45 (2002) 1017–1031.
[21] J. Ahmed, C. Pham-Huu, D. Edouard, A predictive model based on tortuosity for pressure drop estimation in slim and fat foams, Chem. Eng. Sci. 66 (2011) 4771–4779.
[22] X. Yang, T.J. Lu, T. Kim, An analytical model for permeability of isotropic porous media, Phys. Lett. A 378 (2014) 2308–2311.
[23] T. Zhang, X. Li, J. Shi, Z. Sun, Y. Yin, K. Wu, et al., An apparent liquid permeability model of dual-wettability nanoporous media: a case study of shale, Chem. Eng. Sci. 187 (2018) 280–291.
[24] S. Huang, Y. Yao, S. Zhang, J. Ji, R. Ma, A fractal model for oil transport in tight porous media, Transp. Porous Media 121 (2018) 725–739.
[25] Q. Zheng, J. Fan, X. Li, C. Xu, Fractal analysis of the effect of rough surface morphology on gas slip flow in micro- and nano- porous media, Chem. Eng. Sci. 189 (2018) 260–265.
[26] T.A. Cousins, B. Ghanbarian, H. Daigle, Three-dimensional lattice Boltzmann simulations of single-phase permeability in random fractal porous media with rough pore–solid Interface, Transp. Porous Media 122 (2018) 527–546.
[27] Y. Ren, K. Wang, B. Zhu, X. Wang, X. Wang, F. Han, Synthesis of ZnO micro-rods on the cell walls of open celled Al foam and their effect on the sound absorption behavior, Mater. Lett. 91 (2013) 242–244.
[28] Y. Ren, Z. Li, F. Han, Synthesis of Co3O4 micro-needles on the cell walls and their effect on the sound absorption behavior of open cell Al foam, Procedia Mater. Sci. 4 (2014) 191–195.
[29] B. Yu, P. Cheng, A fractal permeability model for bi-dispersed porous media, Int. J. Heat Mass Transf. 45 (2002) 2983–2993.
[30] B. Yu, L.J. Lee, H. Cao, A fractal in-plane permeability model for fabrics, Polym. Compos. 23 (2002) 201–221.
[31] D. Shou, J. Fan, F. Ding, A difference-fractal model for the permeability of fibrous porous media, Phys. Lett. A 374 (2010) 1201–1204.
[32] X. Shen, L. Li, W. Cui, Y. Feng, Improvement of fractal model for porosity and permeability in porous materials, Int. J. Heat Mass Transf. 121 (2018) 1307–1315.
[33] B. Xiao, J. Fan, F. Ding, A fractal analytical model for the permeabilities of fibrous gas diffusion layer in proton exchange membrane fuel cells, Electrochim. Acta 134 (2014) 222–231.
[34] J. Cai, B. Yu, Prediction of maximum pore size of porous media based on fractal geometry, Fractals. 18 (2010) 417–423.
[35] J. Cai, L. Luo, R.A.N. Ye, X. Zeng, X. Hu, Recent advances on fractal modeling of permeability for fibrous porous media, Fractals. 23 (2015) 1540006.
[36] P. Xu, A.P. Sasmito, B. Yu, A.S. Mujumdar, Transport phenomena and properties in treelike networks, Appl. Mech. Rev. 68 (2016) 040802–040817.
[37] A. Majumdar, B. Bhushan, Fractal model of elastic-plastic contact between rough surfaces, J. Tribol. 113 (1991) 1–11.
[38] L. He, J. Zhu, The fractal character of processed metal surfaces, Wear. 208 (1997) 17–24.
[39] Y. Chen, C. Zhang, M. Shi, G.P. Peterson, Optimal surface fractal dimension for heat and fluid flow in microchannels, Appl. Phys. Lett. 97 (2010), 084101.
[40] S. Yang, B. Yu, M. Zou, M. Liang, A fractal analysis of laminar flow resistance in roughened microchannels, Int. J. Heat Mass Transf. 77 (2014) 208–217.
[41] S. Yang, M. Liang, B. Yu, M. Zou, Permeability model for fractal porous media with rough surfaces, Microfluid. Nanofluid. 18 (2015) 1085–1093.
[42] A.H. Meghdadi Isfahani, I. Tasdighi, A. Karimipour, E. Shirani, M. Afrand, A joint lattice Boltzmann and molecular dynamics investigation for thermohydraulical simulation of nano flows through porous media, Eur. J. Mech. B Fluids 55 (2016) 15–23.

[43] H. Liu, Q. Kang, C.R. Leonardi, S. Schmieschek, A. Narváez, B.D. Jones, et al., Multiphase lattice Boltzmann simulations for porous media applications, Comput. Geosci. 20 (2016) 777–805.
[44] X. Wang, K. Procházka, Z. Limpouchová, Partitioning of polymers between bulk and porous media: Monte Carlo study of the effect of pore size distribution, J. Colloid Interface Sci. 567 (2020) 103–112.
[45] B.B. Mandelbrot, B.B. Mandelbrot, The Fractal Geometry of Nature, WH Freeman, New York, 1982.
[46] A. Majumdar, B. Bhushan, Role of Fractal Geometry in Roughness Characterization and Contact Mechanics of Surfaces, 1990.
[47] B. Yu, J. Li, Some fractal characters of porous media, Fractals. 9 (2001) 365–372.
[48] M. Denn, Process Fluid Mechanics, Prentice Hall, 1980.
[49] M.S. Phanikumar, R.L. Mahajan, Non-Darcy natural convection in high porosity metal foams, Int. J. Heat Mass Transf. 45 (2002) 3781–3793.
[50] J.G. Fourie, J.P. Du Plessis, Pressure drop modelling in cellular metallic foams, Chem. Eng. Sci. 57 (2002) 2781–2789.
[51] Y. Pan, G. Xu, W. Li, C. Zhong, A novel numerical cubic filament model and method for the two-energy equation in porous media, Int. J. Heat Mass Transf. 80 (2015) 688–697.
[52] B. Yu, Analysis of flow in fractal porous media, Appl. Mech. Rev. 61 (2008), 050801.
[53] J. Bear, Dynamics of Fluids in Porous Media, Courier Corporation, 2013.
[54] B. Yu, Fractal character for tortuous streamtubes in porous media, Chin. Phys. Lett. 22 (2005) 158.
[55] F.A. Dullien, Porous Media: Fluid Transport and Pore Structure, Academic Press, 2012.
[56] M. Yun, B. Yu, P. Xu, J. Wu, Geometrical models for tortuosity of streamlines in three-dimensional porous media, Can. J. Chem. Eng. 84 (2006) 301–309.
[57] D. Weaire, R. Phelan, The physics of foam, J. Phys. Condens. Matter 8 (1996) 9519.